Optics Letters

Asymmetric dual-loop feedback to suppress spurious tones and reduce timing jitter in self-mode-locked quantum-dash lasers emitting at 1.55 μm

HAROON ASGHAR* AND JOHN G. MCINERNEY

Department of Physics and Tyndall National Institute, University College Cork, Cork, Ireland
**Corresponding author: haroon.asghar@ucc.ie*

Received 1 August 2017; revised 24 August 2017; accepted 27 August 2017; posted 29 August 2017 (Doc. ID 303892); published 15 September 2017

We demonstrate an asymmetric dual-loop feedback method to suppress external cavity side-modes induced in self-mode-locked quantum-dash lasers with conventional single- and dual-loop feedback. In this Letter, we report optimal suppression of spurious tones by optimizing the delay in the second loop. We observed that asymmetric dual-loop feedback, with large (~8×) disparity in loop lengths, gives significant suppression in external-cavity side-modes and produces flat radio frequency (RF) spectra close to the main peak with a low timing jitter, compared to single-loop feedback. Significant reduction in RF linewidth and timing jitter was produced by optimizing the delay time in the second feedback loop. Experimental results based on this feedback configuration validate predictions of recently published numerical simulations. This asymmetric dual-loop feedback scheme provides simple, efficient, and cost-effective stabilization of optoelectronic oscillators based on mode-locked lasers.

OCIS codes: (140.4050) Mode-locked lasers; (140.5960) Semiconductor lasers; (270.2500) Fluctuations, relaxations, and noise.

https://doi.org/10.1364/OL.42.003714

Semiconductor mode-locked diode lasers (MLLs) are compact, rugged, and efficient sources of ultra-short, intense, and high-repetition frequency optical pulses with many potential applications such as all-optical clock recovery, lidar, optical frequency combs, and telecommunications [1–3]. A major limitation of MLLs for most practical applications is their very high timing jitter and phase noise, as spontaneous emission noise and cavity losses make MLLs prone to broad linewidths and, therefore, substantial phase noise [4]. To improve the timing jitter, several experimental methods such as single-cavity feedback [5–8], coupled optoelectronic oscillators [9], injection locking [10–12], and dual-loop feedback [13–15] have been proposed and demonstrated. Of the stabilization techniques demonstrated to date, optical feedback is a promising approach in which an additional reflector creates a compound cavity with a high quality factor, with no need for an external radio frequency (RF) or optical source. Due to the existence of the extra mirror, sidebands resonant with the round-trip time of the external cavity are generated which affect the overall timing jitter and quality of the RF spectra. To overcome these issues, optoelectronic feedback [9] can also be utilized to stabilize the timing jitter and to suppress cavity side-modes by conversion of the optical oscillation (using a fast photodetector) to an electrical signal used in a long feedback loop. This technique does not require an RF source, but requires optical-to-electrical conversion. Recently, a simpler dual-loop feedback technique [13–15] without optical/electrical conversion has been demonstrated to improve timing jitter of the MLLs and to filter or suppress the unwanted spurious side-bands. Dual-loop configuration proposed to date [13,14] yields a sub-kilohertz linewidth, but produces additional noise peaks at frequencies resonant with the inverse of the delay time in the second cavity. This is undesirable in many applications where low noise and flat spectra are required, as in frequency comb generation. Most recently, the influence of the second feedback delay on side-mode suppression [16] and timing jitter [17] has been studied numerically. In this Letter, we report experimental investigation to eliminate these adverse dynamical effects using asymmetric dual-loop feedback by appropriately choosing the length of the second feedback cavity. The best side-mode suppression and lower timing jitter relative to single-loop feedback were achieved with the length ratio between the two cavities ~8×. It was further observed that the RF linewidth and integrated timing jitter were reduced by increasing the length of the second cavity. Our findings suggest that noise stabilization and side-mode suppression depend strongly on additional feedback delay times.

Devices under investigation are two-section InAs/InP quantum-dash mode-locked laser (QDash MLL) with an active layer composed of nine InAs quantum-dash monolayers grown by gas source molecular beam epitaxy embedded within two barriers and separate confinement heterostructure (SCH) layers (dash in a barrier structure). Both barriers and SCH layers consisted of $In_{0.8}Ga_{0.2}As_{0.4}P_{0.6}$ quaternary materials with

$\lambda_g = 1.55$ μm [18]. Total cavity length was 2030 μm with absorber lengths 240 μm (length ratio ~11.8%), giving repetition frequency ~20.7 GHz ($I_{\text{Gain}} = 300$ mA) and average free-space output powers of a few milliwatts. Mode-locking was obtained without reverse bias applied to the absorber section, and the heat sink temperature was fixed at 19°C. This is a two-section device, but works similarly to a single-section self-mode-locked laser, since the absorber is not biased; in this case, the amount of minimal residual absorption does not affect the mode-locking mechanism [12]. The absorber and gain sections were isolated by a resistance >10 k. The QDash MLL was mounted p-side up on a ceramic submount, and copper blocks with active temperature control and electrical contacts were formed by wire bonding.

A schematic for the dual-loop technique is depicted in Fig. 1. For single- and dual-loop feedback configurations, a calibrated fraction of light was fed back through port 1 of an optical circulator, then injected into the laser cavity via port 2. Optical coupling loss from port 2 to port 3 was –0.64 dB. The output of the circulator was sent to a semiconductor optical amplifier (SOA) with gain of 9.8 dB, then split into two arms by a 50/50 coupler. 50% went to an RF spectrum analyzer (Keysight E-series, E4407B) via a 21 GHz photodiode and to optical spectrum analyzers (Ando AQ6317B and Advantest Q8384). The other 50% of power was split into two equal parts by a 3 dB splitter. For a single feedback loop, all power passed through loop-I. For dual-loop configurations (feedback loops-I and-II), the power was split into two loops at the 3 dB splitter. Feedback strengths in both loops were controlled by variable optical attenuators and monitored using the power meter. In this experimental arrangement, the length of loop-I was fixed to 160 m, while the length of second

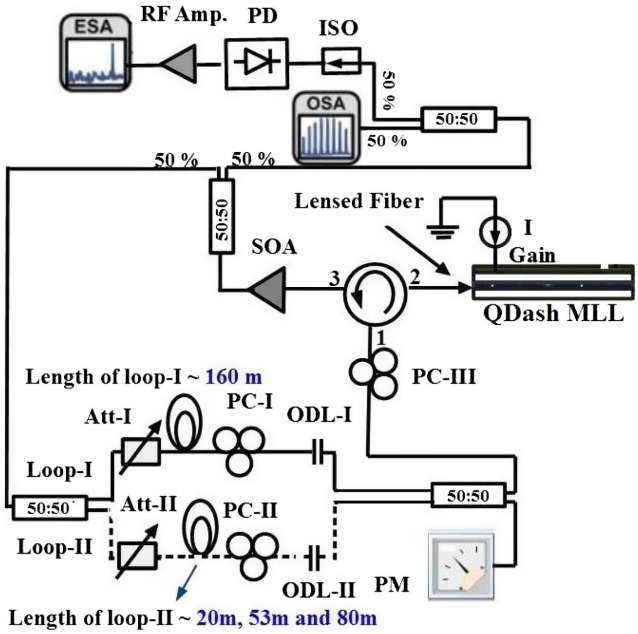

Fig. 1. Schematic of the experimental arrangement for single- (excluding dashed portion) and dual-loop configurations (with dashed portion). SOA, semiconductor optical amplifier; ISO, optical isolator; PD, photodiode; ODL, optical delay line; Att, optical attenuator; PC, polarization controller; ESA, electrical spectrum analyzer; OSA, optical spectrum analyzer; PM, power meter; QDash MLL, quantum-dash mode-locked laser.

feedback loop was varied in three chosen lengths: 20, 53, and 80 m. Polarization controllers (PCs) in each loop, plus one PC before port 1 of the circulator, ensured the light fed back through both loops matched the emitted light polarizations to maximize feedback effectiveness. In this experiment, the feedback ratio into gain section was limited to ~ – 22 dB.

In this Letter, the RMS timing jitter is calculated from the single-sideband (SSB) phase noise spectra measured for the fundamental RF frequency (≈20.7 GHz) using

$$\sigma_{\text{RMS}} = \frac{1}{2\pi f_{ML}} \sqrt{2 \int_{f_d}^{f_u} L(f)\mathrm{d}f}, \tag{1}$$

where f_{ML} is the pulse repetition rate, and f_u and f_d are the upper and lower integration limits. $L(f)$ is the SSB phase noise spectrum, normalized to the carrier power per Hz. To measure the RMS timing jitter of the laser in more detail, SSB noise spectra for the fundamental harmonic repetition frequency were measured. To assess this, RF spectra at several spans around the repetition frequency were measured from small (finest) to large (coarse) resolution bandwidths. The corresponding ranges for frequency offsets were then extracted from each spectrum and superimposed to obtain SSB spectra normalized for power and per unit of frequency bandwidth. The higher frequency bound was set to 100 MHz (instrument limited).

To observe the RF spectrum of single-loop feedback, the length of feedback loop was initially set at 160 m; optimally stable resonance occurred when the feedback length was fine tuned using an optical delay line (ODL-I) (which spanned 0 to 84 ps in steps of 1.67 ps). Such optimization provides a resonant condition (at delay setting = 13 ps) under which the RF linewidth was reduced from 100 kHz free-running to as low as 4 kHz, with an integrated timing jitter to 0.7 from 3.9 ps [integrated from 10 kHz to 100 MHz]. Measured phase noise traces for free-running laser (green line) and single-loop feedback (gray line) as functions of frequency offset from fundamental mode-locked frequency are depicted in Fig. 5. Under similar delay settings, external cavity side-modes appear in the RF spectrum with frequency spacing of 1.28 MHz, the inverse of the loop round-trip delay. RF spectra are shown in Fig. 2(a) (gray line) and Fig. 2(b) (gray line), using spans of 10 and 100 MHz, respectively. Frequency resonances can be seen in both frequency spans which contribute significantly to timing jitter, particularly for the longer feedback cavities, as they are closer to the main peak and are less suppressed [11]. To eliminate these fluctuations and to improve the side-mode suppression ratio, dual-loop feedback was implemented as described in the next section.

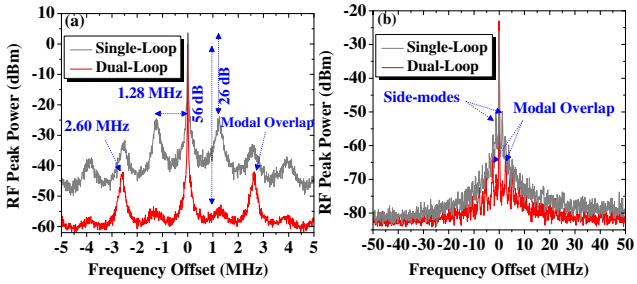

Fig. 2. RF Spectra of single-loop feedback of a length of 160 m (gray line) and dual-loops having lengths of 160 m for loop-I and 80 m for loop-II (red line) using a frequency span of (a) 10 and (b) 100 MHz.

To assess the suppression of these frequency resonances, a shorter feedback cavity corresponding to half the period of noise-induced oscillations of loop-I was introduced. Feedback strengths of both cavities were equalized using variable optical attenuators (Att-I and Att-II), plus fine adjustment of PCs (PC-I and PC-II) in both feedback loops. One optical delay line (ODL-II) was adjusted to full resonance and the length of the other ODL-I was tuned over the maximum range available, 0–84 ps. When ODL-I and ODL-II were fine-tuned (ODL-I = 15 ps and ODL-II = 25 ps) so that every second mode of loop-I coincided precisely with a mode of loop-II; maximum >30 dB suppression in the first-order side-mode was achieved. However, additional noise fluctuations (modal overlap) appeared at frequencies resonant with the inverse of the length of the second delay time which becomes the carrier signal. These noise fluctuations depend on the ratio of the loop lengths. Here, these fluctuations at frequency spacing 2.60 MHz are consistent with the length of the second feedback loop 80 m. RF spectra of asymmetric dual-loop configuration are shown in Fig. 2(a) (red line) and Fig. 2(b) (red line), using spans of 10 and 100 MHz, respectively. In this fully resonant configuration, the RF linewidth narrowed to <1 kHz (instrument limited), with timing jitter reduced to 295 fs. Phase noise traces and RF spectra are shown in the Fig. 5 (blue line) and Fig. 6 (blue line), respectively. The RF spectra illustrated in Figs. 2(a) and 2(b) show that this feedback configuration is not suitable to achieve effective suppression in frequency resonances, as the second delay time will be resonant with the second mode of the first feedback loop which restrict many practical applications where flat and sideband-free RF spectra are required. To improve on this situation, a different dual-loop feedback configuration with non-resonant shorter second loop (53 m) was investigated, described in the next section.

In the dual-loop configuration presented in this section, the length of loop-I was initially set to 160 m, while that of loop-II was 53 m. Upon fine tuning of both ODLs (ODL-I = 13 ps and ODL-II = 15 ps), when the second delay time was resonant with the third harmonic of the first loop, suppression of the first two frequency resonances occurred, while the third harmonic (modal overlap) remained unsuppressed. This harmonic was observed at a frequency offset of 3.9 MHz, corresponding to the 53 m length of the outer feedback loop. RF spectra for the asymmetric dual-loop configuration are shown in Fig. 3(a) (red line) and Fig. 3(b) (red line), using spans 10 and 100 MHz, respectively. In this feedback configuration, when both external feedback cavities are fully resonant, then the RF linewidth narrows to 2 kHz with an integrated timing jitter as low as 0.45 ps. Phase noise trace and RF spectra are

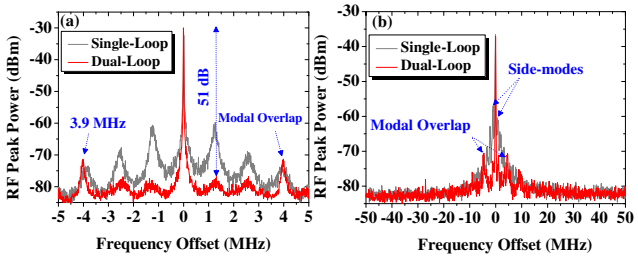

Fig. 3. RF Spectra of single-loop feedback with a length of 160 m (gray line) and dual-loops having lengths of 160 m for loop-I and 53 m for loop-II (red line) using a frequency span of (a) 10 and (b) 100 MHz.

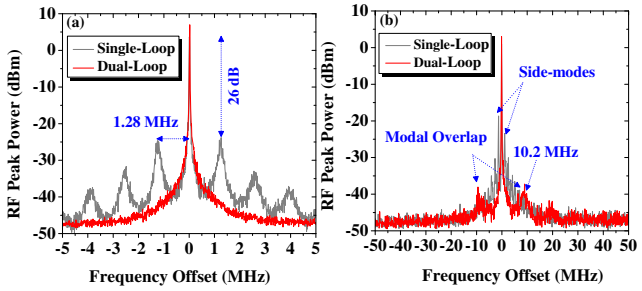

Fig. 4. RF Spectra of single-loop feedback with a length 160 m (gray line) and dual-loops having lengths of 160 m for loop-I and 20 m for loop-II (red line) using a frequency span of (a) 10 and (b) 100 MHz.

shown in Fig. 5 (black line) and Fig. 6 (black line), respectively. These experimentally measured results show that external cavity side-modes cannot be optimally suppressed by simply choosing the second feedback delay time to be a fraction of the first. To achieve stable and flat RF spectra, we designed an asymmetric dual-loop feedback configuration for effective suppression in external cavity side-modes which produced flat RF spectra close to the main peak compared to conventional single- and dual-loop feedback schemes.

In this asymmetric dual-loop feedback configuration the length of loop-I was fixed (160 m), and loop-II was set at ∼8× shorter than loop-I. Fine tuning of both cavities (ODL-I = 15 ps and ODL-II = 21 ps) produced precise coincidence of every eighth mode of loop-I with a mode of loop-II, so that strong side-mode suppression occurred and all feedback-induced side-modes and spectral resonances were eliminated under a frequency span of 10 MHz. RF spectra for this dual-loop feedback configuration (red line) are shown in Figs. 4(a) and 4(b) with frequency spans of 10 and 100 MHz, respectively. It should be noted that the length of loop-II (∼20 m) is only optimal in our specific experimental setup. Further reduction in the length of second feedback loop is not possible, as the combined variable optical attenuator, ODL, PC, and 3 dB coupler have a minimum length of ∼20 m.

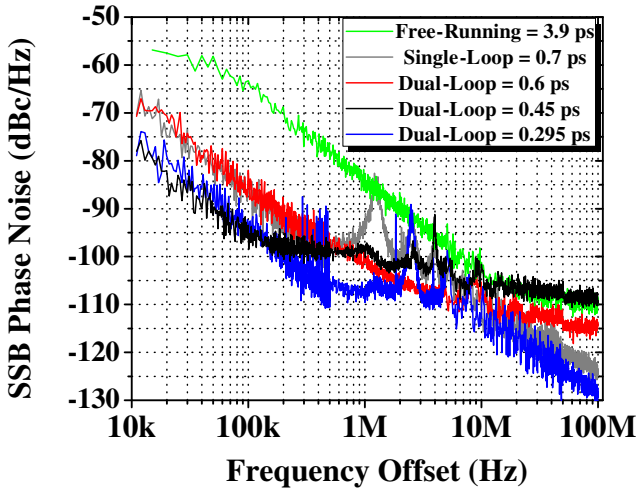

Fig. 5. SSB phase noise trace of free-running, single-loop feedback and dual-loop feedback configurations with loop-I = 160 m and loop-II 20, 53, and 80 m.

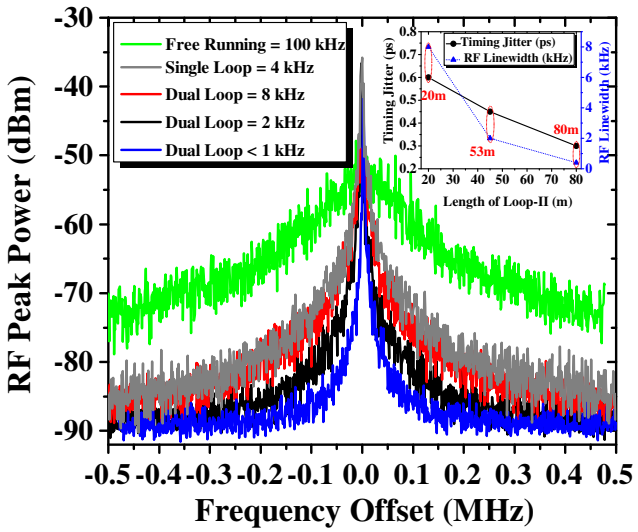

Fig. 6. RF spectra for free-running, single- and dual-loop feedback with loop-I = 160 m and loop-II 20 m (red line), 53 m (black line) and 80 m (blue line); inset shows RF linewidth (blue triangles) and integrated timing jitter (black circles) for dual-loop feedback with loop-I = 160 m and loop-II 20, 53, and 80 m.

Better suppression in external cavity side-modes could be achieved in an arrangement not subject to this limitation, such as photonic integrated circuit. Furthermore, when both external feedback cavities are fully resonant, then the RF linewidth narrows to 8 kHz with an integrated timing jitter 0.6 ps. The phase noise trace and RF spectra are shown in the inset of Fig. 5 (red line) and Fig. 6 (red line), respectively. In this configuration, the RF linewidth was higher than for single-loop feedback, but the measured timing jitter was lower; this is due to suppression of external cavity side-modes. In addition, a weak modal overlap (with intensity ~ – 6 dBm) in the RF spectra of dual-loop feedback was noticed at 10.2 MHz of frequency spacing, consistent with our 20 m outer loop; this is shown in Fig. 4(b) (red line). This behavior shows that effective suppression of external cavity side-modes and reduced timing jitter can be achieved by appropriately fine-tuning the length of the second feedback loop.

Measured phase noise traces for the free-running condition (green line), single-loop feedback (gray line), and dual-loop feedback with loop-II at 20 (red line), 53 (black line), and 80 m (blue line) as functions of frequency offset from the fundamental mode-locked frequency are given in Fig. 5.

Comparison of RF linewidth and integrated timing jitter under stable resonant condition as functions of three chosen lengths of the second feedback cavity is shown in inset of Fig. 6. Measured integrated timing jitter in all dual-loop configurations was lower than for single-loop feedback. However, best suppression in the external cavity side-modes was achieved with the second delay time ~8× shorter than first. Furthermore, the integrated timing jitter in this case was 16% lower than single-loop feedback. Reduction in timing jitter occurs due to suppression of external cavity side-modes relative to single-loop feedback. In the literature [13,14], it was experimentally observed that side-mode suppression was achieved when both feedback delays had a common multiple. This shows that effective suppression in external cavity side-modes is highly dependent on the length of the second loop. Recently, the influence of the second loop delay on suppression of external cavity side-modes [16] and timing jitter [17] was studied numerically. In this Letter, experimental results on suppression of external cavity side-modes and integrated timing jitter as a function of the second cavity delay correspond well with published numerical simulations [16,17].

In summary, an asymmetric dual-loop feedback method has been demonstrated to suppress additional noise resonances in conventional single- and dual-loop feedback setups. These results show that dual-loop feedback with precise alignment of the second loop delay effectively suppresses external cavity side modes and produces flat RF spectra closer to the main peak. Furthermore, by increasing the length of the second loop, significant reduction in the RF linewidth and an integrated timing jitter was produced. Our experimental results have validated recently published numerical simulations. Using this method, stable and sideband-free integrated photonic oscillators based on MLLs can be developed which are feasible and attractive for many applications in optical telecommunications, time-domain multiplexing, frequency comb generation, and as synchronized pulse sources or multi-wavelength lasers for wavelength diversity or multiplexing.

Funding. European Office of Aerospace Research and Development (FA9550-14-1-0204); Science Foundation Ireland (SFI) (12/IP/1658).

REFERENCES

1. A. Sano, E. Yamada, H. Masuda, E. Yamazaki, T. Kobayashi, E. Yoshida, Y. Miyamoto, R. Kudo, K. Ishihara, and Y. Takatori, J. Lightwave Technol. **27**, 3705 (2009).
2. C. J. Misas, P. Petropoulos, and D. J. Richardson, J. Lightwave Technol. **26**, 3110 (2008).
3. S. Fukushima, C. F. C. Silva, Y. Muramoto, and A. J. Seeds, J. Lightwave Technol. **21**, 3043 (2003).
4. F. Kèfèlian, S. O'Donoghue, M. T. Todaro, J. G. McInerney, and G. Huyet, IEEE Photon. Technol. Lett. **20**, 1405 (2008).
5. O. Solgaard and K. Y. Lau, IEEE Photon. Technol. Lett. **5**, 1264 (1993).
6. C.-Y. Lin, F. Grillot, N. A. Naderi, Y. Li, and L. F. Lester, Appl. Phys. Lett. **96**, 051118 (2010).
7. K. Merghem, R. Rosales, S. Azouigui, A. Akrout, A. Martinez, F. Lelarge, G.-H. Duan, G. Aubin, and A. Ramdane, Appl. Phys. Lett. **95**, 131111 (2009).
8. D. Arsenijević, M. Kleinert, and D. Bimberg, Appl. Phys. Lett. **103**, 231101 (2013).
9. X. S. Yao and L. Maleki, J. Opt. Soc. Am. B **13**, 1725 (1996).
10. Y. Cheng, X. Luo, J. Song, T.-Y. Liow, G.-Q. Lo, Y. Cao, X. Hu, X. Li, P. H. Lim, and Q. J. Wang, Opt. Express **23**, 6392 (2015).
11. E. Sooudi, C. D. Dios, J. G. McInerney, G. Huyet, F. Lelarge, K. Merghem, R. Rosales, A. Martinez, A. Ramdane, and S. P. Hegarty, IEEE J. Sel. Top. Quantum Electron. **19**, 1101208 (2013).
12. E. Sooudi, G. Huyet, J. G. McInerney, F. Lelarge, K. Merghem, R. Rosales, A. Martinez, A. Ramdane, and S. P. Hegarty, IEEE Photon. Technol. Lett. **23**, 1544 (2011).
13. M. Haji, L. Hou, A. E. Kelly, J. Akbar, J. H. Marsh, J. M. Arnold, and C. N. Ironside, Opt. Express **20**, 3268 (2012).
14. H. Asghar, E. Sooudi, P. Kumar, W. Wei, and J. G. McInerney, Opt. Express **25**, 15796 (2017).
15. O. Nikiforov, L. Jaurigue, L. Drzewietzki, K. Lüdge, and S. Breuer, Opt. Express **24**, 14301 (2016).
16. L. Jaurigue, E. Schöll, and K. Lüdge, Phys. Rev. Lett. **117**, 154101 (2016).
17. http://dx.doi.org/10.14279/depositonce-5543.
18. F. Lelarge, B. Dagens, J. Renaudier, R. Brenot, A. Accard, F. V. Dijk, D. Make, O. Le Gouezigou, J. Provost, F. Poingt, J. Landreau, O. Drisse, E. Derouin, B. Rousseau, F. Pommereau, and G.-H. Duan, IEEE J. Sel. Top. Quantum Electron. **13**, 111 (2007).